2D ACOUSTIC FULL WAVEFORM INVERSION OF SUBMARINE SALT LAYER USING DUAL SENSOR STREAMER DATA

N. Thiel and T. Bohlen

email: *niklas.thiel@kit.edu*

keywords: *FWI, subsalt imaging, flooding technique, wavefield separation*

ABSTRACT

Our aim is to develop a full waveform inversion (FWI) workflow for subsalt seismic inversion using the flooding technique. In this work we present the results of the very first step of this workflow which is the reconstruction of the salt body. We use a marine field dataset from offshore West Africa, which was recorded with a dual sensor streamer and the receiver ghost removed. For the inversion we apply the two dimensional acoustic full waveform inversion code IFOS2D.

We first verify our approach using synthetic data. Despite of the very complex structure of the salt body in the true model including strong topography and a rough surface we were able to reconstruct the salt layer successfully. The synthetic tests are followed by the first successful inversion results of the field data. Without any a priory information about the salt body in the starting model it was possible to image the surface and bottom of the salt layer.

INTRODUCTION

Hydrocarbons are the most used energy feed stocks in the world. Energy companies are constantly looking for new reservoirs but the discovery of new hydrocarbons becomes increasingly challenging (Leveille et al., 2011). In the past, salt basins proved to be successful sites for the search. The migrated oil and gas is trapped at the bottom of salt layers or at the flanks of salt domes. The Gulf of Mexico (GoM) is probably the most well known site. But also other areas as offshore South-East America or West Africa become more and more interesting (Leveille et al., 2011).

Classical imaging techniques often have problems picturing the salt body or the subsalt region (e.g., Ravaut et al., 2008). The reason for this is the complex shape of most salt bodies and salt layers. The salt was deposited millions of years ago and other sediments deposited on top. The lower density of salt in comparison to the surrounding sediments and the high load allowed the salt to move upwards and formed canopies. This leads to a strong topography of the salt structure. In addition to the shape, the allochthonous salt layers often contain trapped sediments and have a rugose surface (Leveille et al., 2011). The intricate shapes and surfaces of salt bodies result in a complex wave propagation. Regions of poor illumination are often present. Additionally, the energy coming up from subsalt regions is weak due to high reflection coefficients at the sediment-salt interface.

As possible geological misinterpretations are very expensive reliable processing methods must be developed. For smaller salt bodies methods like undershooting and usage of longer offsets lead to good results (e.g. Corcoran et al., 2007). For integrated salt layers even these techniques are not applicable. A promising solution for the problem of subsalt imaging is the application of Full Waveform Inversion (FWI). Unlike conventional techniques the entire waveform is used in the FWI approach. Synthetic data is modelled by using a starting model of the subsurface beneath the acquisition profile. The synthetic data is compared to the field data. In order to match the synthetic data to the field data the starting model is updated iteratively.

By using the full information of the acquired wavefield the FWI can improve the depth image considerably, in particular the subsalt area.

In this work we image a salt layer with a complex structure in a synthetic case study and from field data. To support the inversion and avoid cycle skipping due to a bad starting model we use the flooding technique similar to the one described in Boonyasiriwat et al. (2010). It is a multistage inversion strategy ideal for models with high parameter contrast. No a priori information about the salt body is needed.

FIELD DATA AND MODEL

The used field dataset is part of a 2D marine line from offshore West Africa, delivered by PGS. The data was shot over a continuous salt layer and recorded by a dual-sensor streamer. The delivered data set was already wavefield separated. The advantages and characteristics are described in the following chapters.

The raw data set is a profile with 265 km length and a shot interval of 50 m. For a better handling of the data we limit the model size to the last 88.5 km of the profile and use only every 10th shot. This leads to 155 shots with a shot spacing of 500 m. The streamer was towed in 20 m depth and the first receiver has a distance of 100 m to the source. The last receiver has more than 10 km offset. Thus, 804 traces are recorded per shot. As the water is over 2 km deep and the salt in parts more than 6 km thick we use 12 s of the recording time.

Due to the usage of a two dimensional inversion code we performed a 3D-2D transformation by using the software *lisousi* (Forbriger et al., 2014). Each trace is convolved with $\frac{1}{\sqrt{t}}$ and multiplied by $v\sqrt{t}$ with t as travel time and v as velocity. Also a resampling to 1.2 ms were done to avoid dispersion and instabilities.

PGS provided us with an interpreted detailed velocity model including the salt layer and a smooth background model. The model has a dimension of 88.5 km in x-direction and 12 km in depth direction. For the synthetic test it is used as true model. For the field data inversion we utilise the model for quality control. The grid distance is set to 12.5 m, which results in about 6.8 million grid points for the total model.

INVERSION STRATEGY

In this work we use the the two dimensional FWI code IFOS2D. In order to minimize the computational costs acoustic inversion is performed (e.g. Tarantola, 1984; Köhn, 2011). The code uses the time domain stress-velocity finite-difference formulation on a standard staggered grid for the forward modelling as describe in Bohlen (2002). The gradients are derived by the adjoint state method (Tarantola, 1984). The inversion scheme is shown in figure 2.

In order to quantify the misfit between the real and modelled data the normalised L2-norm is used. It proofed to be more robust for field data than the L2-norm (Choi and Alkhalifah, 2012). The inversion starts at 5 Hz and increases the frequency content during the inversion up to 12 Hz. As the results are mostly from the first few iterations most inverted models were inverted with a frequency content of 5 Hz maximum.

To decrease the influence of noise on the inversion result and therefore the appearance of artefacts the field seismograms are muted before the first arrival. Important for a successful inversion is also the wavefield used for the forward simulation. Therefore, the source time function is inverted before every frequency step. The inverted wavelets show a high similarity with the source wavelet provided by PGS.

The density model is not inverted. After every flooding a new density model is calculated from the velocity model by using the Gardner relation (Gardner et al., 1974).

WAVEFIELD SEPARATION

For the marine measurements PGS uses dual sensor streamers, also called geostreamers. This kind of streamer can record the pressure as well as the vertical velocity. By combining these two data sets the receiver ghost can be removed from the data. Thus, the notches in the frequency spectrum introduced by the receiver ghost are removed. This can improve the bandwidth of the data significantly. Further benefits in the acquisition are the possible deeper towing of the streamer. The effect of the deeper towed streamer increases the low frequency content in the data (Carlson et al., 2007). This fact makes this method interesting for the FWI. The lack of low frequencies are one of the major problems in the FWI. A further benefit is the higher depth penetration resulting from the lower frequencies and the higher weather independency.

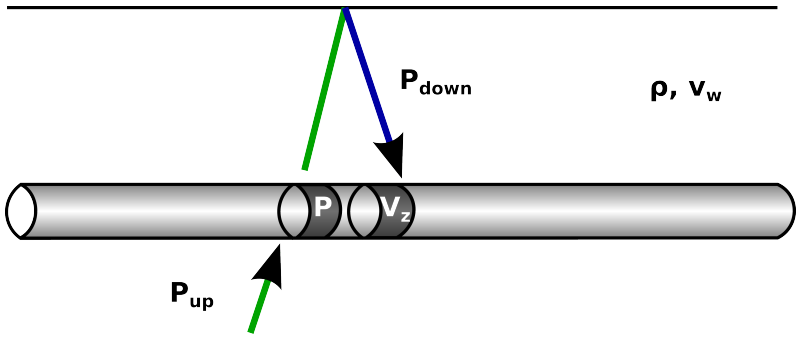

Figure 1: Dual sensor streamer.

The total pressure wavefield P can be divided into an up-going wavefield P_{up} and a down-going wavefield P_{down} (Amundsen, 1993) as pictured in figure 1:

$$P = P_{up} + P_{down} \tag{1}$$

with

$$P_{up} = \frac{1}{2}(P - FV_z) \qquad \text{and} \qquad P_{down}\frac{1}{2}(P + FV_z). \tag{2}$$

V_z is the vertical velocity and F the scaling filter depending on the angular frequency ω, the density ρ and the vertical component of the wavenumber vector k_z:

$$F = \frac{\rho\omega}{k_z} \tag{3}$$

where k_z can be expressed in 2D as follows (Klüver et al., 2008):

$$k_z = \sqrt{\left(\frac{\omega}{v_w}\right)^2 - k_x^2} \tag{4}$$

with v_w as the acoustic wave propagation velocity in water and k_x as horizontal inline component of the wavenumber vector.

The FWI is based on a misfit calculation and backpropagation of the residuals. Therefore, the field data and forward modelled data must be comparable. As the field data was delivered already as P_{up} wavefield we also need to perform the wavefield separation on the forward modelled data. Thus, the wavefield separation was implemented in the FWI workflow directly after the forward modelling and before the misfit calculation. Therefore, at every receiver location the pressure and velocity data must be saved. In figure 2 can be seen that the wavefield separated field data is now comparable with the also wavefield separated forward modelled data (green boxes). The new implemented part is marked with a red box.

The most cost intensive part in terms of computational time is the 2D Fast Forward Transformation (FFT) of the seismograms. Due to a full parallelised implementation in the code of the 2D FFT and the also cost intensive computation of the filter the calculation is as effective as possible.

RESULTS OF SYNTHETIC INVERSION TEST

In the synthetic test we used as starting model the true model without the salt layer. The inversion result after only one iteration can be seen in figure 4(a). For a better visibility of the changes we calculated a difference plot (inverted model - starting model) displayed in figure 4(b). In this plot the salt surface is displayed very clearly in most parts which makes it easy to pick. For instance the maxima of the salt topography or smooth plateaus as at around $x = 55$ km. Not very good visible are steep slopes. Due to the low frequency of 5 Hz the lower part of the valleys are not illuminated well. Also the very rough surface at $x = 34 - 42$ km smears the structure we want to pick in the inversion result. This reveals also the challenge

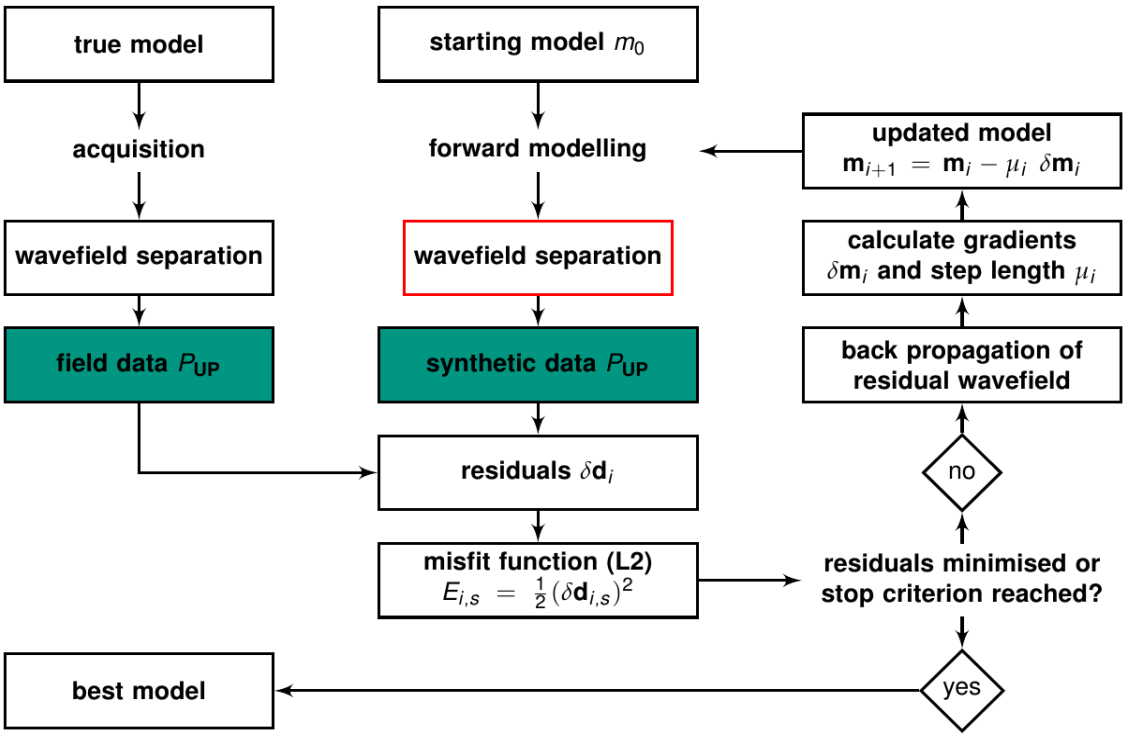

Figure 2: FWI scheme, wavefield separation (red box) included.

of the complex topography of salt layers. From the comparison of the inverted and true model we could calibrate our picking for the field data, especially for the difficult parts.

The picked salt surface was flooded and smoothed. It is shown in figure 4(c), where also the salt surface of the true model is plotted. Except of the edges of the model the salt surface could be reconstructed with an error of about ± 100 m. As we used frequencies only up to 5 Hz for the inversion we have wavelength of about 500 m, which shows the good result of the inversion despite the fact of the complex topography.

The model in figure 4(c) was used as starting model for the next inversion stage, the inversion of the bottom of the salt layer. After only 10 iteration we could pick the salt bottom from the difference plot in figure 6(a). The areas where the salt layer is shallower and thinner as between $x = 60 - 80$ km had higher updates and were good selectable. In the parts between $x = 0 - 60$ km the velocity contrast is much lower. Additionally, the thickness of the salt is high and the structures are located in a high depth at around 8 km. This lead to only small updates in this region. Nevertheless, by comparing the inverted model with the true model in figure 6(c) a good according can be seen. As we focused on the salt layer the step in the sediments was not picked or flooded separately. Therefore, this structure was not inverted very accurately. However, we were able to pick the salt bottom also in this area after only 10 iterations with an error of less than 500 m (about half a wavelength) in most parts. This show the high potential of this method for the subsalt imaging.

RESULTS OF FIELD DATA INVERSION

Despite of the availability of a interpreted model from PGS we started from zero and used the provided PGS model only as quality control for our inversion and picking result. Therefore, the first step was to reproduce the sea floor. For this we used a homogeneous starting model with the water velocity of 1500 $\frac{\mathrm{m}}{\mathrm{s}}$. From the inversion result we picked the water bottom (figure 3(b)). In figure 3(b) the flooded sediments below the picked water bottom is displayed. The also plotted sea floor line of the 'true' model shows the high accuracy of the picking. In addition this test verifies the correctness of the acquisition geometry for the forward modelling.

In figure 5(a) the result after one iteration of the inversion using the starting model in figure 3(b) is plotted. For the better picking the salt surface was picked in the difference plot showed in figure 5(b). It can be seen that the picked salt surface follows the same contour as in the 'true' model. Only the depth is slightly smaller especially in the middle part of the model between $x = 25 - 40$ km. This might be an effect of the low frequencies which reduce the accuracy. Also the weathering of the salt surface can influence the beginning of the salt layer. A high roughness of the surface smears the selectable structures as we have already seen in the previous chapter. The greatest differences are about 400 m, which is less than one wavelength in the sediments at 5 Hz. Also the deep valleys cannot be picked in the inversion result due to the lack of high frequencies. Furthermore, some structures at a depth of about 4 km and between profile length 70-90 km are inverted, not visible in the 'true' starting model.

The plot figure 7(a) shows the difference plot of the inversion result after 22 iterations minus the starting model (figure 5(c)). As in the synthetic test the subsalt structure is hard to pick, but the structures are visible, especially the flanks of the valleys of the salt. At the shallower area on the right side of the model the updates are higher and more clearly. In this area we were able to pick along one minimum of a structure in the difference plot.

After picking the model was flooded below the picked line with sediment velocity analogue to the synthetic test. We also did not pick the step in the sediments despite the visibility in the difference plot due to the focusing on the salt body. The comparison of the inverted salt bottom with the line of the PGS model show high similarities. The rough structure is the same. The combination of flooding technique and FWI seems to be very effective in imaging the salt body in only few iterations. Moving to higher frequencies should improve the resolution considerably.

CONCLUSIONS & OUTLOOK

Our results indicate that FWI is able to image the sea bottom as well as the top salt interface. The latter is required for the application of the Flooding Technique allowing also the inversion of subsalt structures. Further tests with a better imaging of the shallow area below the seabed and the usage of higher frequencies will be the next step to get a higher resolution of the overburden which will in turn also improve the subsalt reconstruction.

ACKNOWLEDGEMENTS

We thank PGS for providing the data set and model. This work was kindly supported by the sponsors of the *Wave Inversion Technology (WIT) Consortium*. We gratefully acknowledge the computing time granted on the supercomputer JURECA at Jülich Supercomputing Centre (JSC).

REFERENCES

Amundsen, L. (1993). Wavenumber-based filtering of marine point-source data. *Geophysics*, 58(9):1335–1348.

Bohlen, T. (2002). Parallel 3-D viscoelastic finite difference seismic modelling. *Computers & Geosciences*, 28(8):887–899.

Boonyasiriwat, C., Schuster, G. T., Macy, B., Valasek, P., and Cao, W. (2010). Application of multi-scale waveform inversion to marine data using a flooding technique and dynamic early-arrival windows. *Geophysics*, 75(6):R129–R136.

Carlson, D., Long, A., Söllner, W., Tabti, H., Tenghamn, R., and Lunde, N. (2007). Increased resolution and penetration from a towed dual-sensor streamer. *First Break*, 25(12).

Choi, Y. and Alkhalifah, T. (2012). Application of multi-source waveform inversion to marine streamer data using the global correlation norm. *Geophysical Prospecting*, 60:748–758.

Corcoran, C., Perkins, C., Lee, D., Cattermole, P., Cook, R., and Moldoveanu, N. (2007). A wide-azimuth streamer acquisition pilot project in the gulf of mexico. *The Leading Edge*, 26(4):460–468.

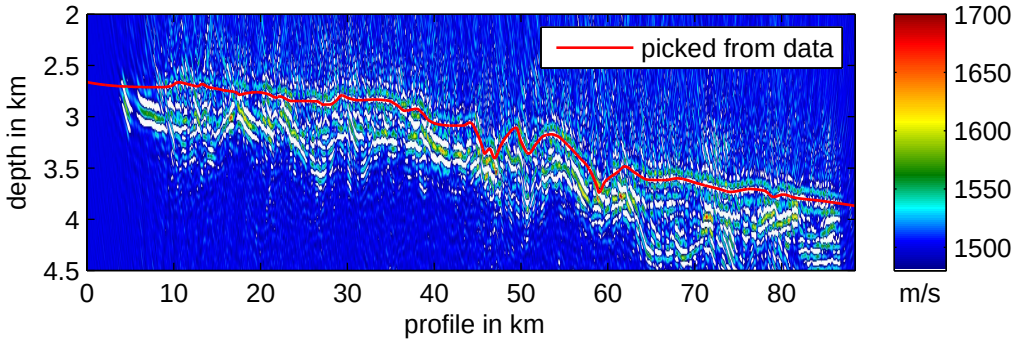

(a) Inversion result after 10 iterations with picked water bottom.

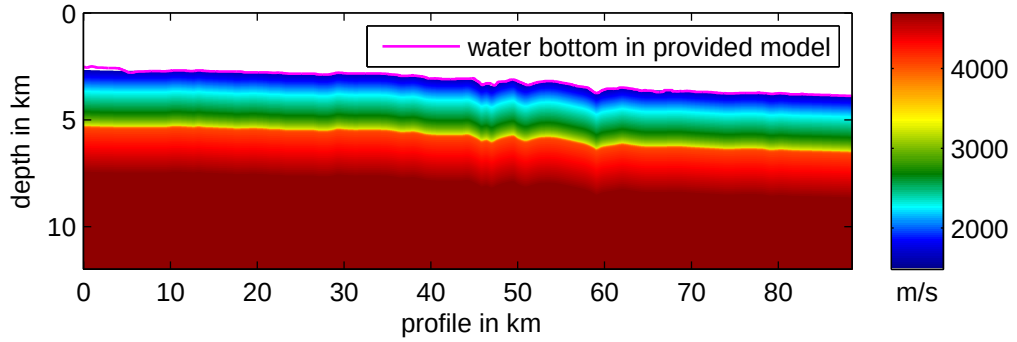

(b) Flooded sediments after inversion and picking of water bottom.

Figure 3: Field data inversion: V_P models after inversion for water bottom. Starting model was a homogeneous fullspace with water velocity.

Forbriger, T., Groos, L., and Schäfer, M. (2014). Line-source simulation for shallow-seismic data. part 1: Theoretical background. *Geophysical Journal International*, 198(3):1387–1404.

Gardner, G. H. F., Gardner, L. W., and Gregory, A. R. (1974). Formation basics for velocity and density - the traps diagnostic stratigraphic. *Geophysics*, 39(6):770–780.

Klüver, T. et al. (2008). Wavefield separation for dual-sensor data with local handling of aliased energy. In *2008 SEG Annual Meeting*. Society of Exploration Geophysicists.

Köhn, D. (2011). *Time Domain 2D Elastic Full Waveform Tomography*. PhD thesis, Christian-Albrechts-Universität zu Kiel.

Leveille, J. P., Jones, I. F., Zhou, Z.-Z., Wang, B., and Liu, F. (2011). Subsalt imaging for exploration, production, and development: A review. *Geophysics*, 76(5):WB3–WB20.

Ravaut, C., Alerini, M., Pannetier-Lescoffit, S., and Thomassen, E. (2008). Sub-salt imaging by full-waveform inversion: a parameter analysis. In *2008 SEG Annual Meeting*.

Tarantola, A. (1984). Inversion of seismic reflection data in the acoustic approximation. *Geophysics*, 49(8):1259–1266.

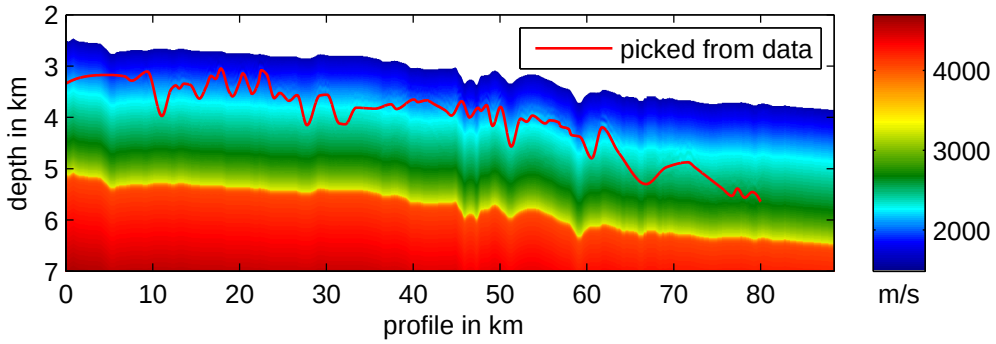

(a) Inversion result after 1 iterations with picked salt surface.

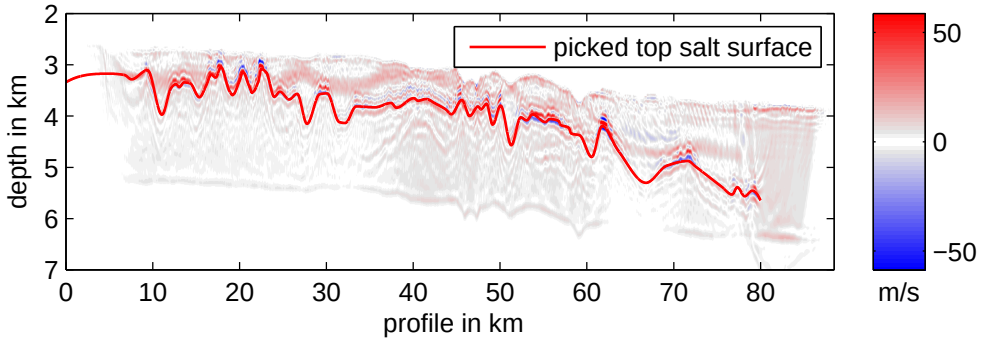

(b) Difference plot of inversion result after 1 iteration - starting model.

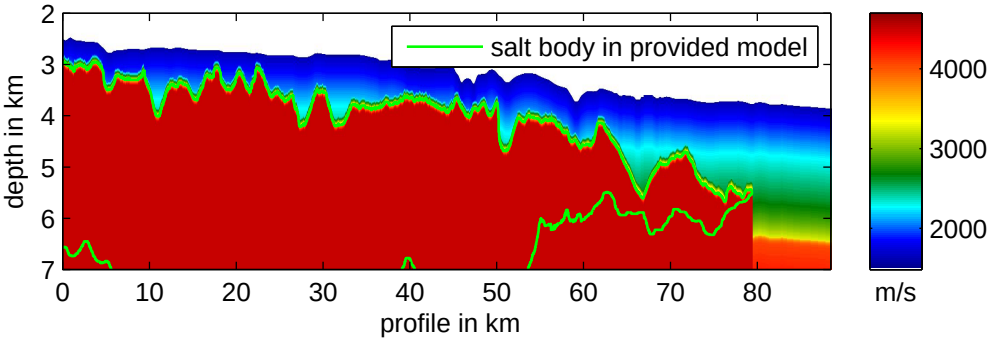

(c) Flooded salt after inversion and picking of salt surface.

Figure 4: Synthetic inversion: V_P models after inversion for salt surface.

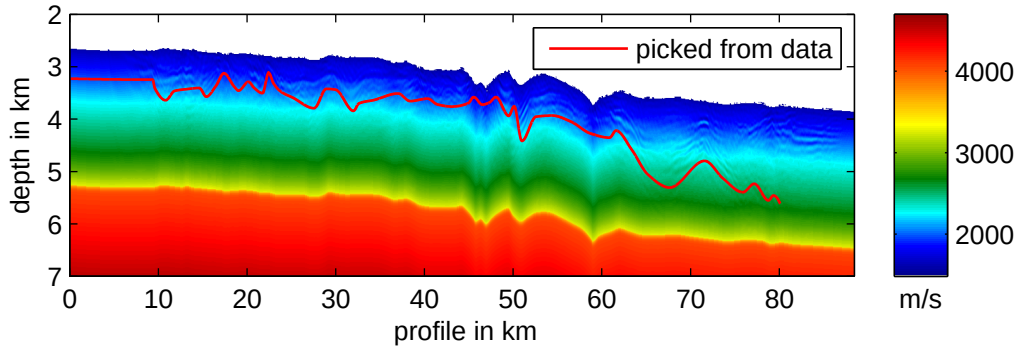

(a) Inversion result after 2 iterations with picked salt surface.

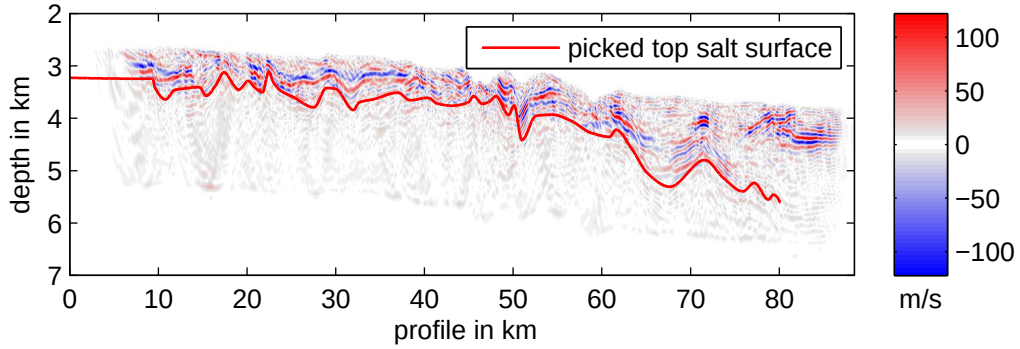

(b) Difference plot of inversion result after 2 iteration - starting model (figure 3(b)).

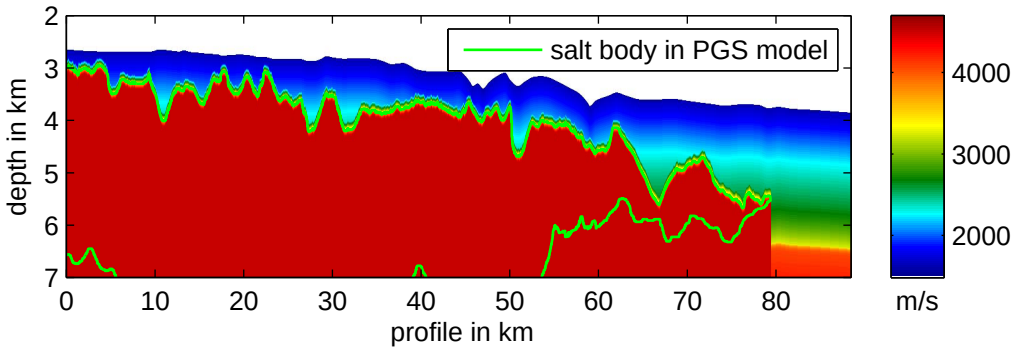

(c) Flooded salt after inversion and picking of salt surface.

Figure 5: Field data inversion: V_P models after inversion for salt surface. Starting model was the model in figure3(b).

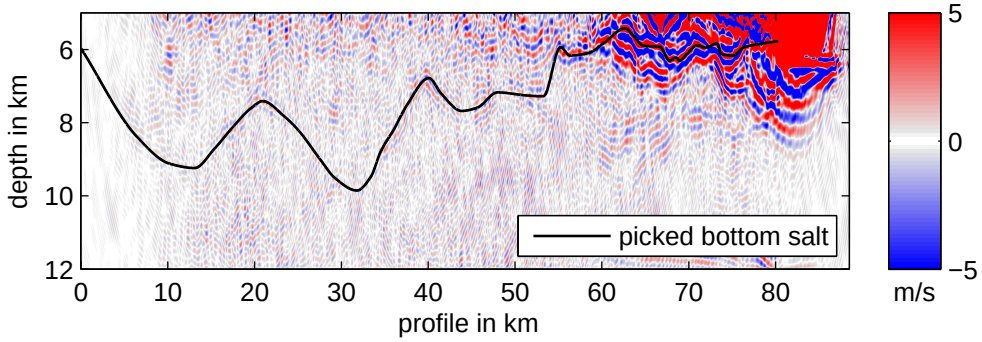

(a) Difference plot of inversion result after 10 iteration - starting model (figure 4(c)).

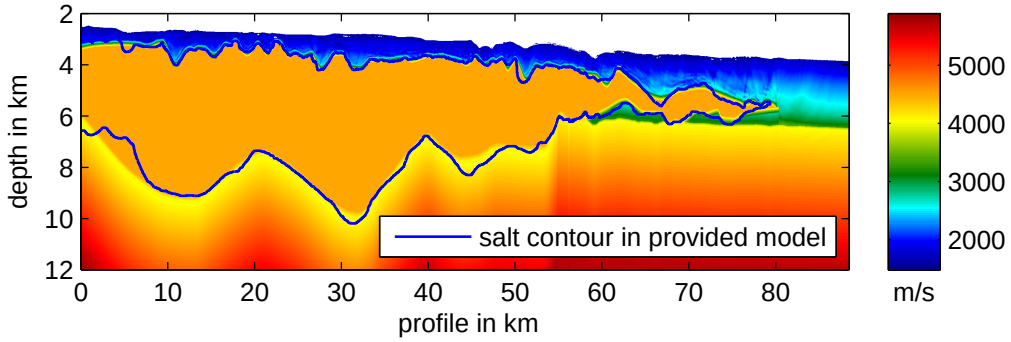

(b) Flooded sediments after inversion and picking of salt bottom.

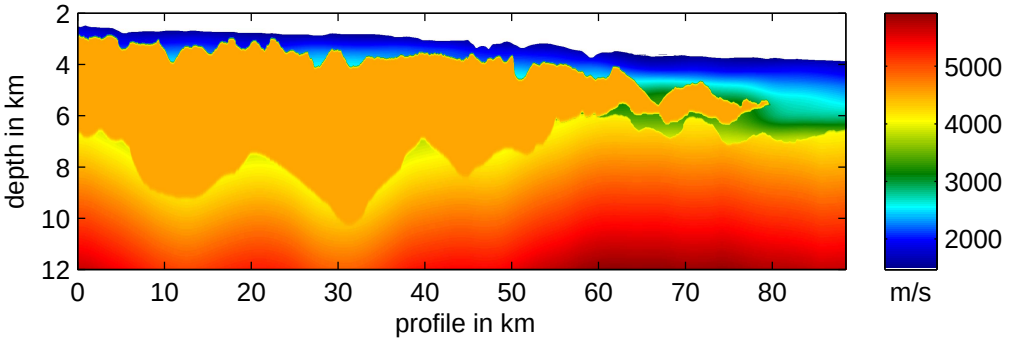

(c) True vp model.

Figure 6: Synthetic inversion: V_P models after inversion for salt bottom.

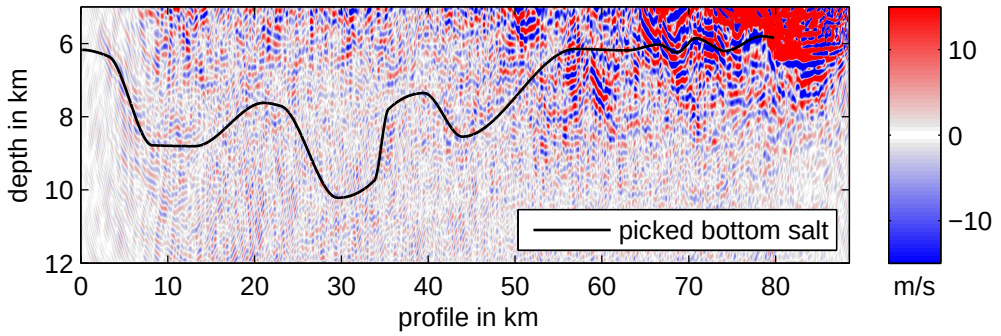

(a) Difference plot of inversion result after 22 iteration - starting model (figure 4(c)).

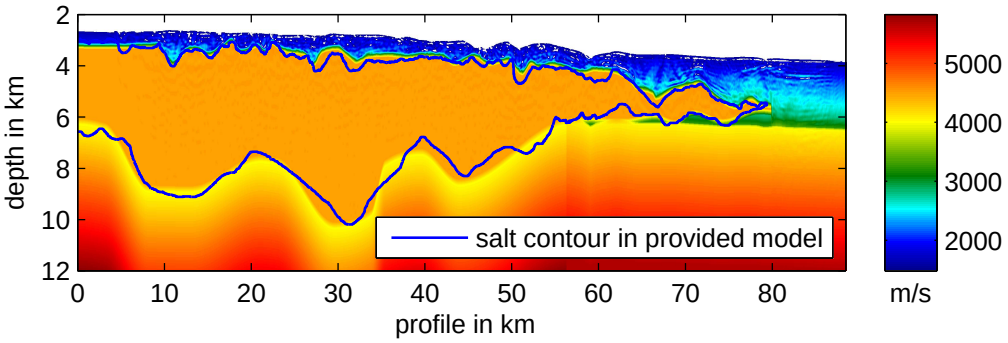

(b) Flooded sediments after inversion and picking of salt bottom.

Figure 7: Field data inversion: V_P models after inversion for salt bottom.